Impact of Concrete-Encased Grounding Systems on Lightning Overvoltages in Transmission Lines

W. L. M. de Azevedo, T. F. G. Pascoalato, A. R. J. de Araújo, S. Kurokawa, J. Pissolato Filho

***Abstract*—This paper addresses the influence of concrete on the overvoltages developed in a 138-kV transmission line (TL) subjected to lightning strikes with variable amplitude. This study considers a tower-footing grounding system consisting of four counterpoise conductors, utilizing both bare and concrete-encased electrodes. The harmonic grounding impedance is initially calculated over a frequency range from 100 Hz to 10 MHz. Subsequently, the ground potential rise (GPR) developed by the tower-footing grounding system under lightning currents with adjustable peak values is analyzed. Furthermore, the impulse impedance is computed to model the tower-footing grounding system within the simulated power network. The TL is modeled using the Universal Line Model (ULM), which incorporates frequency-dependent (FD) soil parameters and ground-return parameters calculated via Nakagawa's equations. Simulations are performed in ATP-EMTP, where the ULM is implemented in MATLAB and incorporated into the model via a PCH file. Finally, the overvoltage waveforms generated for the 138-kV power system subjected to a lightning strike are analyzed for three different values of low-frequency soil resistivity modeled using Alípio-Visacro's approach: 700, 1,500, and 4,000 Ω.m. The simulation results reveal a substantial reduction in harmonic impedance for the concrete-encased grounding system compared to the bare-electrode configuration. This reduction leads to lower impulse impedance and results in GPR waveforms with significantly reduced peak values when concrete is incorporated into the grounding system. However, in high-resistivity soils, the reduction achieved by the concrete-encased system is limited to approximately 33%. In addition, the overvoltages generated by lightning strikes are lower when the concrete-encased grounding system is used. In contrast, the bare grounding system leads to backflashover events, which do not occur when the concrete-encased grounding system is used.**

***Keywords*—Concrete, electromagnetic transients, grounding system, lightning, transmission lines.**

I. Introduction

One of the measures to mitigate the probability of backflashover occurrence in high-voltage transmission lines is to reduce the tower-footing grounding impedance. Various techniques have been used in the literature, such as additional electrodes, longer conductors, soil treatment, or the addition of low resistivity materials around the grounding system [1], [2]. Concerning the last alternative, the use of bentonite and concrete has recently received significant attention from researchers. In [2], the authors conducted an experimental investigation using vertical electrodes buried in untreated soil and backfilled with a low-resistivity material, assuming the conductors were fully and partially embedded in a commercial aggregate compound. The results demonstrated a significant reduction (more than 20%) in the harmonic impedance of the electrodes, making this an interesting material to replace the grounding system of the transmission towers. Other researchers have conducted computer simulation studies using the finite element method (FEM) to calculate the harmonic (and also impulse) impedances of grounding systems (vertical rods and horizontal electrodes) embedded in concrete, such as in [1], [3]. Regarding the grounding impedance computation, many approaches have been proposed in the literature to model electrodes, based on: (i) lumped and distributed parameters using the transmission line theory [4]; (ii) electromagnetic approach to solve Maxwell's equations solved by numerical methods using full-wave electromagnetic software, such as Method of Moments (MoM) [5], [6], [7], Finite Element Method (FEM) [1], [3], Hybrid Electromagnetic Model (HEM) [8], [9]; (iii) hybrid approaches, such as the Partial Equivalent Element Circuit (PEEC) [10], [11]. To the best of the author's understanding, the existing literature has not examined an analysis of backflashover occurrence in a high-voltage TL with a concrete-encased tower-footing grounding system.

This paper investigates overvoltages generated by lightning strikes, assuming a tower-footing grounding system composed of bare and concrete-encased counterpoise electrodes. First, the harmonic impedance of the tower-footing grounding system is calculated for both bare and concrete-encased electrodes buried in low-frequency soils of 700, 1,500, and 4,000 Ω.m using the full-wave electromagnetic FEKO/Altair Engineering software, employing the Method of Moments (MoM) over a frequency range of 100 Hz to 10 MHz [7]. Next, the Ground Potential Rise (GPR) and impulse impedance are computed for the lightning current of the first return stroke with a peak value of 45 kA, multiplied by factors of 0.5, 1.0, 1.5, and 2.0. Finally, a power system consisting of five transmission towers is simulated using ATP-EMTP software, where TLs are modeled considering the ground-return parameters calculated with the Nakagawa's approach, incorporating frequency-dependent soil parameters in its formulation. The simulation results demonstrate that incorporating concrete into the grounding system significantly reduces its harmonic impedance compared to the traditional bare-electrode configuration. Consequently, the resulting GPR

This work was supported by the Coordenação de Aperfeiçoamento de Pessoal de Nível Superior (CAPES)-Finance code 001 and by São Paulo Research Foundation (FAPESP) (grants: 2021/11258-5, 2020/10141-4 and 2022/09182-3). T. F. G. Pascoalato and S. Kurokawa are with São Paulo State University (UNESP), Ilha Solteira, Brazil. (E-mail: tfg.pascoalato@unesp.br, sergio.kurokawa@unesp.br).

W. L. M. de Azevedo, A. R. J. de Araújo and J. Pissolato Filho are with University of Campinas, Campinas, Brazil. (E-mail of corresponding author: ajaraujo@unicamp.br). (E-mail: w157573@dac.unicamp.br, pisso@unicamp.br).

Paper submitted to the International Conference on Power Systems Transients (IPST2025) in Guadalajara, Mexico, June 8-12, 2025.

waveforms and impulse impedance are considerably lower than those associated with systems utilizing bare electrodes. Moreover, the overvoltages induced in the power system during lightning strikes are remarkably reduced, with lower peak values observed when a concrete-encased grounding system is employed. Results show that a concrete-encased grounding system effectively mitigates the probability of backflashover events, offering enhanced protection for the power system against lightning strikes. As contribution, this paper demonstrates that concrete can be an excellent alternative as a grounding-enhancing compound, effectively reducing the harmonic impedance of the grounding system and mitigating transient overvoltages generated by lightning strikes in power systems.

II. Power system modeling

A. Transmission line

The longitudinal impedance $\boldsymbol{Z}_{\text{long}}(\omega)$ and transversal admittance $\boldsymbol{Y}_{\text{trans}}(\omega)$ of n-phase transmission line (TL), are given by

$$\boldsymbol{Z}_{\text{long}}(\omega) = \boldsymbol{Z}_{\text{int}}(\omega) + \frac{j\omega\mu_0}{2\pi}\left[\ln\left(\frac{D_{\text{ij}'}}{d_{\text{ij}}}\right) + \boldsymbol{S}_1\right], \tag{1}$$

$$\boldsymbol{Y}_{\text{trans}}(\omega) = j\omega\left\{\frac{1}{2\pi\varepsilon_0}\left[\ln\left(\frac{D_{\text{ij}'}}{d_{\text{ij}}}\right) + \boldsymbol{S}_2\right]\right\}^{-1}, \tag{2}$$

being

$$\boldsymbol{S}_1 = 2\int_0^\infty \frac{e^{-(h_\text{i}+h_\text{j})\lambda}}{\sqrt{\lambda^2+\gamma_1^2-\gamma_0^2}+\lambda}\cos(r_{\text{ij}}\lambda)d\lambda, \tag{3}$$

$$\boldsymbol{S}_2 = 2\int_0^\infty \frac{e^{-(h_\text{i}+h_\text{j})\lambda}}{\sqrt{\lambda^2+\gamma_1^2-\gamma_0^2}+\frac{\gamma_1^2}{\gamma_0^2}\lambda}\cos(r_{\text{ij}}\lambda)d\lambda, \tag{4}$$

$$\gamma_1^2 = j\omega\mu_0(\sigma_\text{g} + j\omega\varepsilon_\text{r}\varepsilon_0), \quad \gamma_0^2 = -\omega^2\mu_0\varepsilon_0, \tag{5}$$

where ω [rad/s] is the angular frequency, f is the frequency [Hz], $\boldsymbol{Z}_{\text{int}}(\omega)$ [Ω/m] is the internal impedance related to the *Skin Effect* being modeled by the Bessel's functions [12]. The $D_{\text{ij}'}$ [m] is the distance between the conductor i and the image of adjacent conductor j, d_{ij} [m] is the distance between conductors i and j. The ρ_g is the soil resistivity ($\rho_g = 1/\sigma_g$), being σ_g is its conductivity. The μ_0 [H/m] is the vacuum magnetic permeability ($\mu_0 = 4\pi\times10^{-7}$ H/m), ε_r is the relative permittivity and ε_0 [F/m] is the vacuum permittivity ($\varepsilon_0 = 8.85\times10^{-12}$ F/m).

The terms $\boldsymbol{S}_1$ and $\boldsymbol{S}_2$ are the correction matrices related to the ground-return parameters. This paper calculates the ground-return parameters using Nakagawa's approach because it includes the frequency-dependent soil parameters and the displacement currents [13]. The variables h_i and h_j are the heights of the conductors i and j measured from the ground level [m], r_{ij} is the horizontal distance between the conductors i and j [m], λ is an integration variable. Finally, the soil is characterized by its conductivity σ_g [S/m] and relative permittivity ε_r.

B. Soil modeling

The soil can be represented by its frequency-dependent conductivity σ_g and relative permittivity ε_r, assuming its magnetic permeability equal to the vacuum [14]. Alípio and Visacro in [15] proposed a model to obtain frequency-dependent σ_g and ε_r, given by [15]

$$\sigma_\text{g}(f) = \sigma_0 + \sigma_0\times h(\sigma_0)\left(\frac{f}{1\text{MHz}}\right)^\xi, \tag{6}$$

$$\varepsilon_\text{r}(f) = \frac{\varepsilon'_\infty}{\varepsilon_0} + \frac{\tan(\pi\xi/2)\times10^{-3}}{2\pi\varepsilon_0(1\text{MHz})^\xi}\sigma_0\times h(\sigma_0)f^{\xi-1}, \tag{7}$$

where, σ_0 is the soil conductivity [mS/m] at low frequencies (measured at 100 Hz), and the variables $h(\sigma_0)$, ξ, and $\varepsilon'_\infty/\varepsilon_0$ are detailed in [15].

C. Tower-footing grounding system

Figure 1 shows the tower footing grounding system. Based on this topology, the harmonic grounding impedance (HGI) behavior of the concrete-encased counterpoise is calculated for a large frequency range, varying from 100 Hz to 10 MHz. For this purpose, the grounding system is built in the full-wave electromagnetic software FEKO/Altair Engineering, where its grounding impedance is calculated employing the numerical method of Moments (MoM) [7]. In this software, the HGI can be calculated by:

$$Z(\omega) = \frac{V(\omega)}{I_{\text{ind}}(\omega)}, \tag{8}$$

where frequency domain variables $V(\omega)$ and $I_{\text{ind}}(\omega)$ are the voltage applied in the grounding system and the current induced in the conductor, respectively. It is applied a voltage of $V_\text{s}(\omega) = 1\angle\underline{0^\circ}$ V at the indicated point in Figure 1-(b) and (c), denoted as *port* (marked as a red/blue sphere this figure. Figure 1-(d) details the mesh discretization used during the simulation. The harmonic impedance $Z(\omega)$ is approximated by a rational function, using the *Vector Fitting* method, being generically written as [16]

$$Z(s) \approx Z_{\text{fit}}(s) = \sum_{k=1}^{n}\left(\frac{c_\text{k}}{s+a_\text{k}}\right) + b' + d's \tag{9}$$

where $s = j\omega$ [rad/s] is the complex angular frequency, c_k is the residue, and a_k is the pole. The d' and b' are real constant numbers, and n is the number of poles [16]. The developed potential due to an injected impulse current is denoted as Ground Potential Rise (GPR), being defined as [17]

$$v(t) = \mathscr{F}^{-1}\{Z_{\text{fit}}(s)\times I(s)\} = z_{\text{fit}}(t) * i(t) \tag{10}$$

where $\mathscr{F}^{-1}$ is the inverse Fourier transform and (*) is the convolution between the two functions. The right side of (10) can be solved by using the numerical recursive convolution method as detailed in [18]. Finally, the tower footing impedance is represented by a pure resistance denoted as the impulse impedance (Z_p), calculated by [19]

$$Z_\text{p} = \frac{V_\text{p}}{I_\text{p}} \tag{11}$$

where V_p and I_p are the peak values of the transient GPR and injected current $i(t)$, respectively. The advantage of Z_p

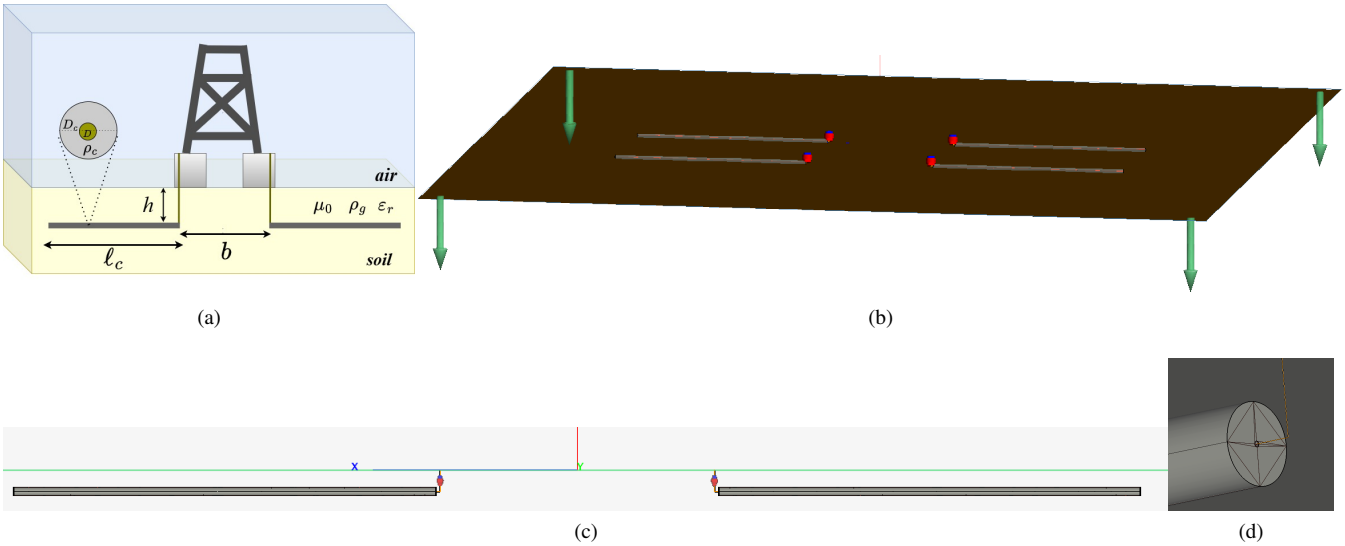

Fig. 1: Counterpoise in the full-wave software FEKO: (a) Tower-footing grounding system; (b) 3-D view; (c) Side view; (d) detail of the earthing electrode encased with concrete and mesh discretization. (Not to scale)

is its concise representation as a lumped resistance for the tower-footing grounding system, which yields similar results to those obtained using the harmonic grounding impedance calculated over a wide frequency range. Furthermore, Z_p, as a lumped parameter, allows for much easier incorporation into EMTP-type platforms compared to the complex circuits derived from the Vector Fitting technique. [20], [21].

D. Lightning current

The lightning current is representative of the first return stroke (FRS) which is a more realistic lightning behavior based on several measurements. The FRS is modeled by a summation of m Heidler's functions and characterized by a double-peak waveform, given by [22]

$$i(t) = \sum_{k=1}^{m} \frac{I_{0k}}{\eta_k} \frac{(t/\tau_{1k})^{n_k}}{1 + (t/\tau_{1k})^{n_k}} e^{-t/\tau_{2k}}, \tag{12}$$

$$\eta_k = e^{\left[-\left(\frac{\tau_{1k}}{\tau_{2k}}\right)\left(n_k \frac{\tau_{2k}}{\tau_{1k}}\right)\right]^{1/n_k}}, \tag{13}$$

where I_{0k} is the peak current amplitude of the k^{th} component, τ_{1k} and τ_{2k} are the time constants that controls the rise time and decay time of the waveform, respectively. The η_k is a normalization factor for the current peak value, and n_k is a shape factor determining the waveform slope. The parameters for the lightning current of FRS with its seven terms ($m = 7$) and its adjustable factors are given by [23]

$$I_{0k} = \alpha\,[6 \quad 5 \quad 5 \quad 8 \quad 16.5 \quad 17 \quad 12]\ [\text{kA}], \tag{14a}$$

$$\tau_{1k} = [3 \quad 3.5 \quad 4.8 \quad 6 \quad 7 \quad 70 \quad 12]\ [\mu s], \tag{14b}$$

$$\tau_{2k} = [76 \quad 10 \quad 30 \quad 26 \quad 23.2 \quad 200 \quad 26]\ [\mu s], \tag{14c}$$

$$n_k = [2 \quad 3 \quad 5 \quad 9 \quad 30 \quad 2 \quad 14] \tag{14d}$$

where α is an adjustable parameter that modifies the values of I_{p1}, I_{p2} of the FRS [23]. The lightning current waveforms in time domain, and its derivatives, adopted in this paper are shown in Fig. 2. According to this figure, the current amplitude increases with increasing adjustable α, along with its maximum value of the derivatives. These characteristics are crucial for overvoltage analysis, as discussed further in detail.

E. Universal Line Model

The Universal Line Model (ULM) is a widely used model to accurately simulate the behavior of TLs and cables in power systems, particularly under transient disturbances, such as lightning surge studies, switching transients, electromagnetic interference (EMI) analysis, directly in the phase domain. This ULM is based on the solution of the Telegrapher's equations, which the rational approximations of the characteristic admittance $\mathbf{Y}_c(s)$ and propagation function $\mathbf{H}(s)$ are obtained using the *Vector Fitting* technique which consist of an approximation of these frequency-dependent admittances by rational functions based on residues, poles and real constants developed by [16]. This model may also incorporate the frequency-dependent soil parameters into the functions $\mathbf{Y}_c(s)$ and $\mathbf{H}(s)$, thereby enabling the coherent representation of high-frequency propagation phenomena and transient analysis [24]. In this study, the authors implemented the procedure outlined in [25] with certain modifications. Initially, the TL parameters, time delays, and *Vector Fitting* for the $\mathbf{Y}_c(s)$ and $\mathbf{H}(s)$ functions were developed as a programming script in MATLAB. Subsequently, a data file was generated to ensure full compatibility with the latest ATP-EMTP (ATPDraw 7.5) [26]. The PCH component was utilized to construct an equivalent circuit, enabling the calculation of transient voltages directly in the time domain in the ATP-EMTP.

III. Numerical Results

A. Grounding system analysis

Numerical simulations were carried out considering the FD soil electrical parameters (ρ_g and ε_g) for bare and concrete-encased electrodes buried in homogeneous grounds

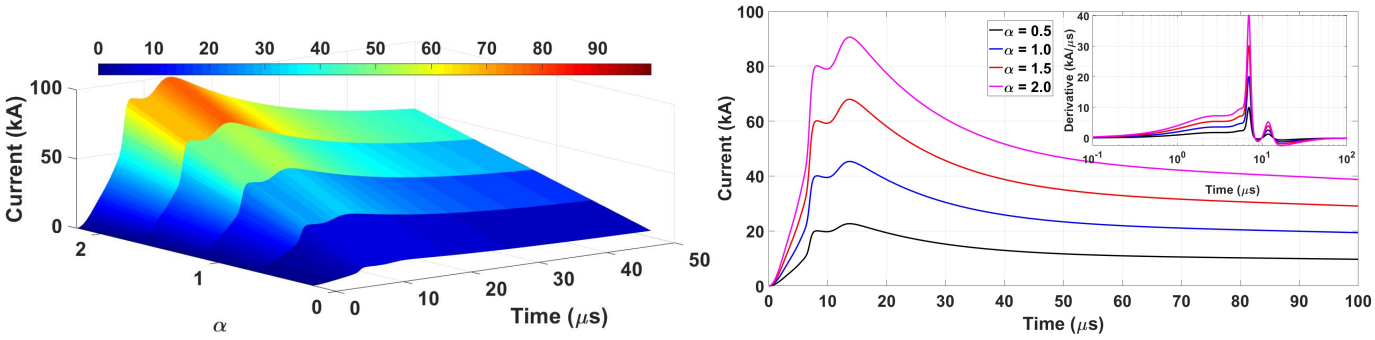

(a) (b)

Fig. 2: Lightning current waveforms of the FRS for α varying from 0.5 to 2: (a) 3-D surface and (b) 2-D lightning waveforms and their derivatives.

for three low-frequency resistivities ρ_0 of 700, 1,500 and 4,000 Ω.m using the model proposed in (6) and (7). The length of the counterpoise electrode ($\boldsymbol{\ell_c}$) is 20 m, a rod radius r of 12.5 mm, the distance between the tower feet (b) of 6.50 m and a depth h of 0.50 m. The concrete-encased electrodes have a radius r_c of 10 cm, and concrete resistivity ρ_c of 30 Ω.m was assumed, based on [1]. The harmonic grounding impedance (HGI) is assessed in the frequency range of 100 Hz to 10 MHz (100 points logarithmically spaced). The HGI computed for the considered grounding system with bare and concrete-encased counterpoise is plotted in Fig. 3.

According to this figure, the low-frequency soil resistivity remarkably affects the HGI across the frequency range. Overall, at the lower frequencies (below 1 kHz), the HGI behaves primarily as a pure resistance, being directly proportional to the low-frequency soil resistivity ρ_0. Furthermore, electrodes with concrete exhibit lower low-frequency resistance than those obtained with bare electrodes. As the frequency increases, the reactive behavior becomes prominent, exhibiting either inductive or capacitive behavior. The HGI decreases with increasing frequency, reflecting a predominance of capacitive behavior, typical of high-resistive soils [1], between 10 kHz to around 1 MHz. This reduction occurs due to the resulting lower equivalent resistivity when added concrete is much lower than the natural medium. Above 5 MHz, the inductive behavior becomes more prominent, increasing as the frequency becomes higher.

B. Ground Potential Rise and Impulse Impedance

The GPR developed for the lighting current of FRS assuming α of 0.5, 1.0, 1.50 and 2.0 are plotted in Fig. 4. According to this figure, the GPR peak increases with increasing soil resistivity. However, those GPR waveforms related to the concrete-encased counterpoise electrodes have presented lower peak values due to the lower harmonic impedance obtained for the concrete-encased grounding system compared to the bare grounding system.

The calculated impulse impedance employing (11) for the tower-footing grounding system with bare and concrete-encased electrodes are shown in Table I. This table shows that the impulse impedance obtained for the bare ground system is higher than those assessed with the concrete-encased electrodes. The impulse impedance rises with the increasing soil resistivity where the percentage difference tends to be around 33%, as a result of the reduction of the harmonic impedance shown in Fig. 3-(a) at the higher frequencies (above 1 MHz), which converges to the close values at this range. It is worth noting that the GPR peak values increase proportionally with increasing α, since the current peaks are also directly proportional and the ratio between V_p/I_p is kept practically constant for all investigated values explored in this paper.

C. Overvoltage analysis

The FRS is modeled as a current source with variable amplitude associated with a channel resistance of 400 Ω injected at the tip of the tower structure. The tower presents its phase conductors located in the positions denoted as A*, B*, and C*, and ground wire **S**, as depicted in Fig. 5-(a). The tower is represented by the multi-conductor model where each section is modeled by a lossless single line with an equivalent surge impedance of Z_{eqi} associated with a propagation velocity (v = 0.85c, c = 300 m/μs), as depicted in Fig. 5-(b). The values of Z_{eqi} are shown in the figure and adopted from [27]. The per-unit-length resistance of phase conductors is 0.21 Ω/km, and for the ground wire is 2.175 Ω/km [28]. The outer radius of the phase conductors is 1.829 cm. The radius of the shield wire is 0.476 cm and the sag in the phase conductors was not considered in the developed MATLAB code. The tower-footing grounding impedance for bare and concrete-encased counterpoise is represented by the impulse impedance Z_p whose values are organized in Table I. The power system is modeled in ATP-EMTP, as illustrated in Fig. 5-(c). The case study comprises five transmission towers with four spans of 400 m. In order to avoid the impact of the reflected waves, two 20-km lines are connected beyond the

TABLE I: Impulse impedance Z_P (Ω) for bare and concrete-encased GS and percentage difference

ρ_g [Ω.m]	Bare Rod	Concrete-Encased	Difference (%)
700	11.31	7.60	32.87
1,500	22.40	14.90	33.47
4,000	50.24	33.35	33.60

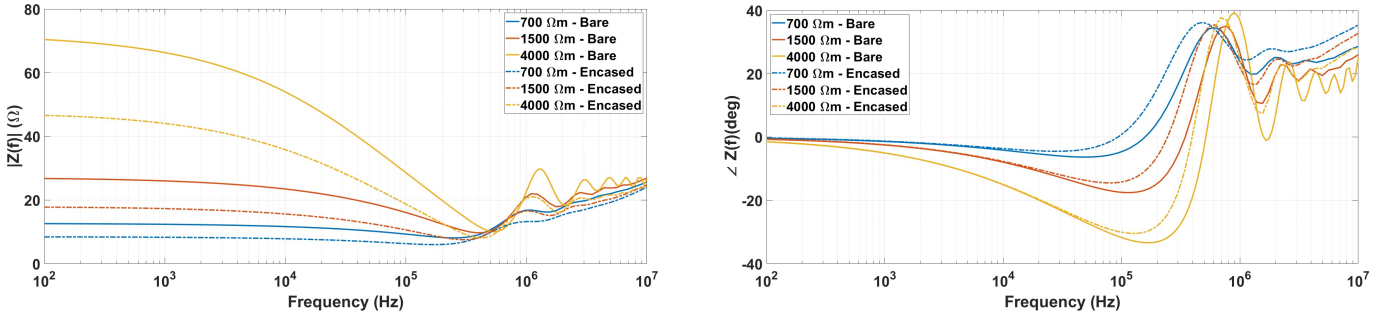

(a) (b)

Fig. 3: Harmonic grounding impedance of the bare and concrete-encased GS: (a) Magnitude; (b) Phase.

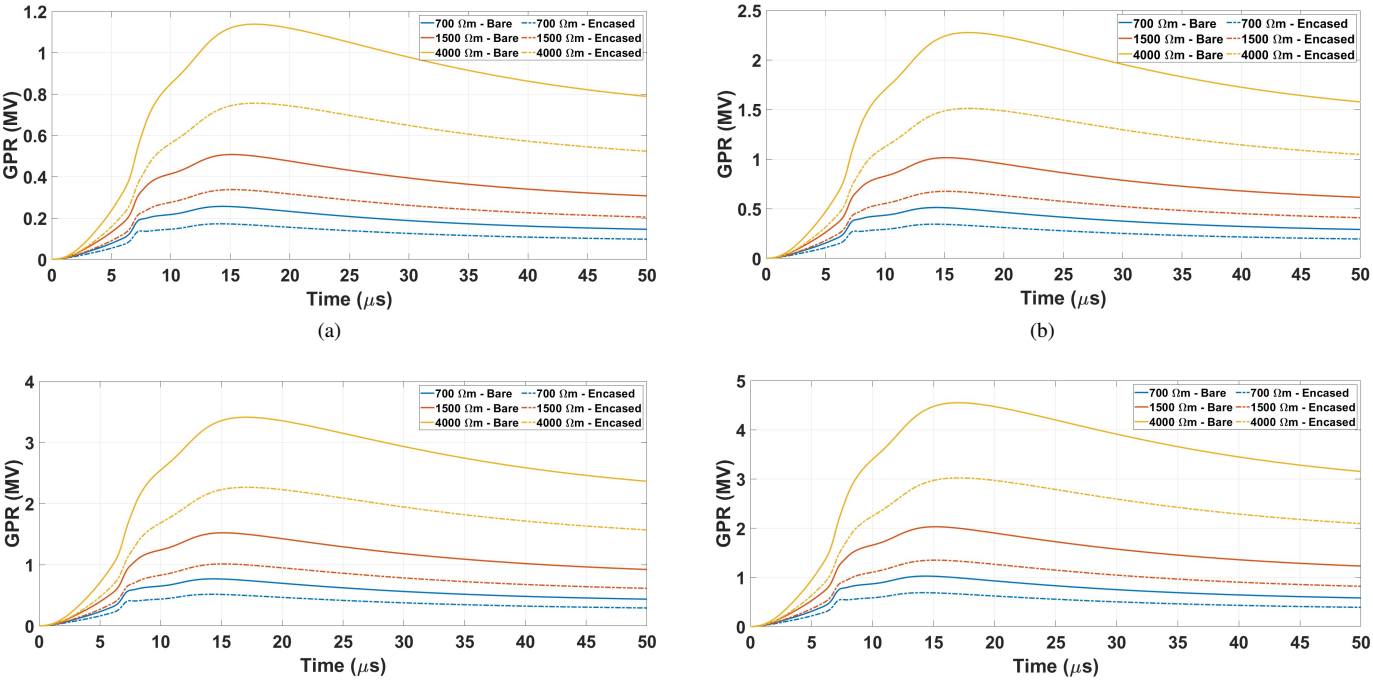

(a) (b) (c) (d)

Fig. 4: Transient GPR for several values of α in the FPI: (a) α = 0.50; (b) α = 1.0;(c) α = 1.50; (d) α = 2.0.

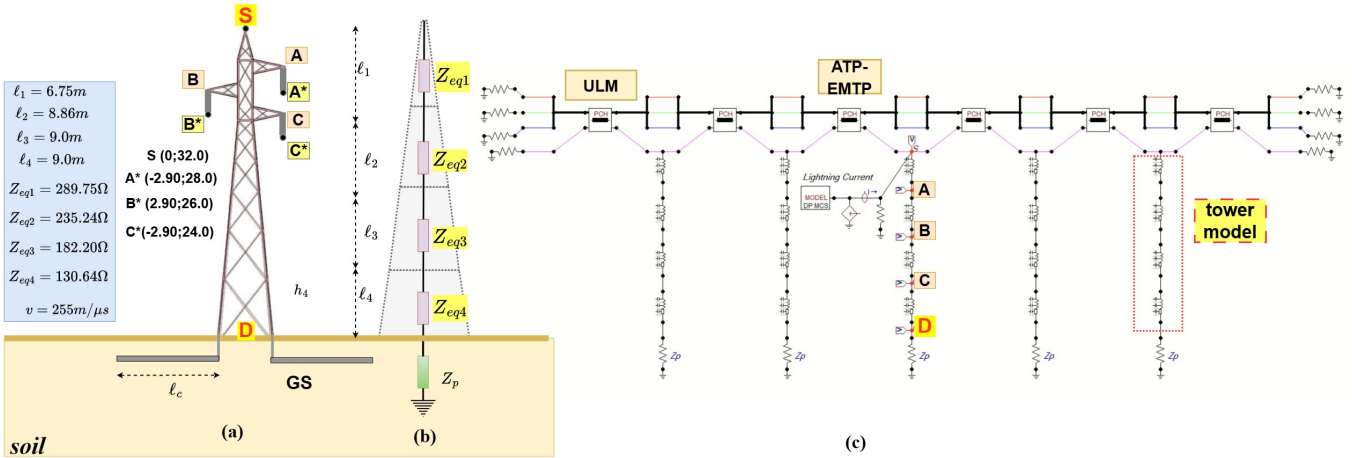

(a) (b) (c)

Fig. 5: (a) Transmission tower configuration-Adapted from [27]; (b) Multi-conductor tower model; (c) Circuit model in ATP-EMTP.

spams and resistive loads of 300 Ω are inserted at the end points of each conductor. The simulations were performed assuming a time step of 10 ns. The insulator string is modeled using the disruption method denoted as the volt-time curve ($V \times t$), expressed by [29]

$$V_{\mathrm{i}}(t) = \left(k_1 + \frac{k_2}{t^{0.75}}\right) \ell_s \tag{15}$$

where k_1 and k_2 are coefficients, ℓ_s [m] is the length of the insulator, and t [μs] is the time after the lightning strikes at the tower. The following parameters are adopted: ℓ_s = 1.56m, k_1 = 400, and k_2 = 710 [29]. If the overvoltage across the insulator string (between A-A*, B-B*, C-C*) is equal to or surpasses the $V \times t$ curve at any given instant, a backflashover (BF) takes place [30]. It is worth mentioning that the volt-characteristic curve is a simplified flashover model, that considers if the flashover occurs at any instant for the overvoltage waveform generated for a certain lightning current. Other insulator flashover models, such as the integration method (disruptive effect method) or Leader progression (LP) model can be investigated in future works[31]. The *pch* file represents the *Transmission Line Model* for each line's span, which takes into account a more realistic soil modeling, assuming its FD electrical parameters proposed by (6) and (7). Furthermore, the ULM incorporates the ground-return parameters (impedance and admittance) using Nakagawa's approach, which considers displacement currents in the soil. The overvoltages generated at the cross-arms, related to the points A, B, C, and GPR at the tower base (point D) assuming the two types of tower-footing grounding systems and FRS with several adjustable factors α are depicted in Fig. 6 where the numbering I, II and III represents the columns associated to the soils of 700, 1,500 and 4,000 Ω.m, respectively. According to this figure, the overvoltage waveforms' behavior significantly depends on the soil resistivity (impulse impedance) and lightning current waveforms. It is noted that there are significant differences between the overvoltages when concrete-encased grounding systems (lower impulse impedance) are considered (dashed lines) compared with those computed for the bare grounding system (higher impulse impedance) shown in the solid lines. Furthermore, the voltage curve $V_{\mathrm{i}}(t)$ (dashed blue light line) intersects with the overvoltages developed in the cross-arms depending on the adjustable factor, presence of concrete-encased electrodes, and soil resistivity. The occurrence of backflashover, denoted as BFs and red dots, are shown in Fig. 6 [see sub-figures (III-b), (I,II,III)-(c) and (I,II,III)-(d)].

The peak values of each overvoltage waveform and the occurrence of the BF are organized in Table II. According to this table, the peak values of the overvoltages and the GPR increase with increasing α and soil resistivity, however, they decrease considerably when the concrete-encased grounding system is employed. For adjustable α of 0.5, there is no BF for both types of grounding systems for all soil resistivities considered. However, as the adjustable α increases, the probability of BF also increases, especially associated with the soil of 4,000 Ω.m. For α = 2.0, all simulations resulted in BF, since the highest injected current of I_{p} = 2 × 45 kA = 90 kA is considered. It is interesting to observe that assuming concrete-encased tower footing yields no backflashover occurrence, which considering the bare conductors for tower footing results in backflashover, as seen in Fig. 6 [see I-(c), II-(d), II-(c)]. The values of the percentage difference $\epsilon(\%)$ are calculated by

$$\epsilon(\%) = \frac{V_{\mathrm{p}}^{\mathrm{bare}} - V_{\mathrm{p}}^{\mathrm{concrete}}}{V_{\mathrm{p}}^{\mathrm{bare}}} \times 100\%, \tag{16}$$

where $V_{\mathrm{p}}^{\mathrm{bare}}$ and $V_{\mathrm{p}}^{\mathrm{concrete}}$ represent the peak values of the overvoltages for bare and concrete-encase grounding system, respectively, along the tower point P = {A, B, C, D}. The calculated percentage difference is organized in Table III. As seen in this table, point A has the lower percentage difference for every soil resistivity, since this point is the closest to the lightning injection point (point S in Fig. 5). However, the percentage difference at points D and C is slightly smaller for soil with a resistivity of 4,000 Ω·m than 1,500 Ω·m. This occurs because the impulse impedance Z_p is not proportional to the increase in soil resistivity for both bare and concrete-encased rods, as shown in Table I. This is due to the harmonic grounding impedance [see Fig.3], where the capacitive effect is much more pronounced in soil with a resistivity of 4,000 Ω· m at higher frequencies. In contrast, for soil with a resistivity of 700 Ω·m, the inductive behavior predominates across the entire frequency range. Additionally, the propagation effect becomes more significant at the lower points of the tower (points C and D) due to the greater distance traveled by the wave current from the injection point S. Point D has shown the highest peak percentage difference for each soil resistivity and adjustable factor α, up to 29.8%. This variation is caused by higher propagation time combined with the higher attenuation of the traveling wave to reach the tower base.

The overvoltage percentage differences do not depend on α because Z_p, represented as a constant resistance at the tower footing, generates overvoltages tend to be approximately proportional to the adjustable factor α for the injected lightning current and its respective GPR. This significant difference in lightning overvoltages impacts the probability of backflashover, which can result in outages in power systems. The simulation results further suggest that concrete is an advantageous low-resistivity material for mitigating backflashover occurrences in transmission lines exposed to lightning strikes.

IV. Conclusions

This paper examines the influence of concrete on the tower-footing grounding systems and on grounding performance and overvoltage waveforms in a power network generated by lightning strikes with increasing current peak. Simulation investigations were conducted assuming adjustable factors of 0.5, 1.0, 1.50 and 2.0 times the lightning current peak and three different soils, modeled using Alípio-Visacro's approach, with three different low-frequency resistivities. The harmonic grounding impedance (HGI) was found to be primarily resistive at low frequencies. However, as the frequency increases, the reactive component

TABLE II: Peak values (MV) of the overvoltages at points A, B and C with occurrence of backflashover for each phase (Y-yes or N-no) and GPR in point D

Bare tower-footing grounding system																
	α = 0.5				α = 1.0				α = 1.5				α = 2.0			
ρ_g(Ω.m)	**A**	**B**	**C**	**D**	**A**	**B**	**C**	**D**	**A**	**B**	**C**	**D**	**A**	**B**	**C**	**D**
700	0.324(N)	0.256(N)	0.208(N)	0.201	0.47(N)	0.511(N)	0.416(N)	0.402	0.971(Y)	0.767(N)	0.625(N)	0.603	1.295(Y)	1.023(Y)	0.833(N)	0.804
1,500	0.449(N)	0.393(N)	0.367(N)	0.364	0.898(N)	0.785(N)	0.733(N)	0.729	1.346(Y)	1.178(Y)	1.100(Y)	1.093	1.795(Y)	1.571(Y)	1.466(Y)	1.457
4,000	0.719(N)	0.696(N)	0.691(N)	0.690	1.438(Y)	1.392(Y)	1.382(Y)	0.380	2.157(Y)	2.088(Y)	2.072(Y)	2.070	2.875(Y)	2.783(Y)	2.763(Y)	2.760
Concrete encased tower-footing grounding system																
	α = 0.5				α = 1.0				α = 1.5				α = 2.0			
ρ_g(Ω.m)	**A**	**B**	**C**	**D**	**A**	**B**	**C**	**D**	**A**	**B**	**C**	**D**	**A**	**B**	**C**	**D**
700	0.279(N)	0.208(N)	0.154(N)	0.143	0.558(N)	0.415(N)	0.308(N)	0.287	0.837(N)	0.623(N)	0.462(N)	0.430	1.116(Y)	0.831(N)	0.616(N)	0.574
1,500	0.366(N)	0.301(N)	0.261(N)	0.256	0.732(N)	0.603(N)	0.522(N)	0.511	1.098(Y)	0.904(N)	0.782(N)	0.767	1.464(Y)	1.205(Y)	1.043(Y)	1.023
4,000	0.562(N)	0.520(N)	0.507(N)	0.506	1.124(Y)	1.040(Y)	1.014(Y)	1.012	1.687(Y)	1.560(Y)	1.522(Y)	1.518	2.249(Y)	2.080(Y)	2.029(Y)	2.024

TABLE III: Percentage difference $\epsilon(\%)$ for the overvoltages in the power system

Bare tower-footing grounding system																
	α = 0.5				α = 1.0				α = 1.5				α = 2.0			
ρ_g(Ω.m)	**A**	**B**	**C**	**D**	**A**	**B**	**C**	**D**	**A**	**B**	**C**	**D**	**A**	**B**	**C**	**D**
700	13.8	18.8	26.0	28.6	13.8	18.8	26.0	28.6	13.8	18.8	26.0	28.6	13.8	18.8	26.0	28.6
1,500	18.5	23.2	28.8	29.8	18.5	23.2	28.8	29.8	18.5	23.2	28.8	29.8	18.5	23.2	28.8	29.8
4,000	21.8	25.3	26.6	26.7	21.8	25.3	26.6	26.7	21.8	25.3	26.6	26.7	21.8	25.3	26.6	26.7

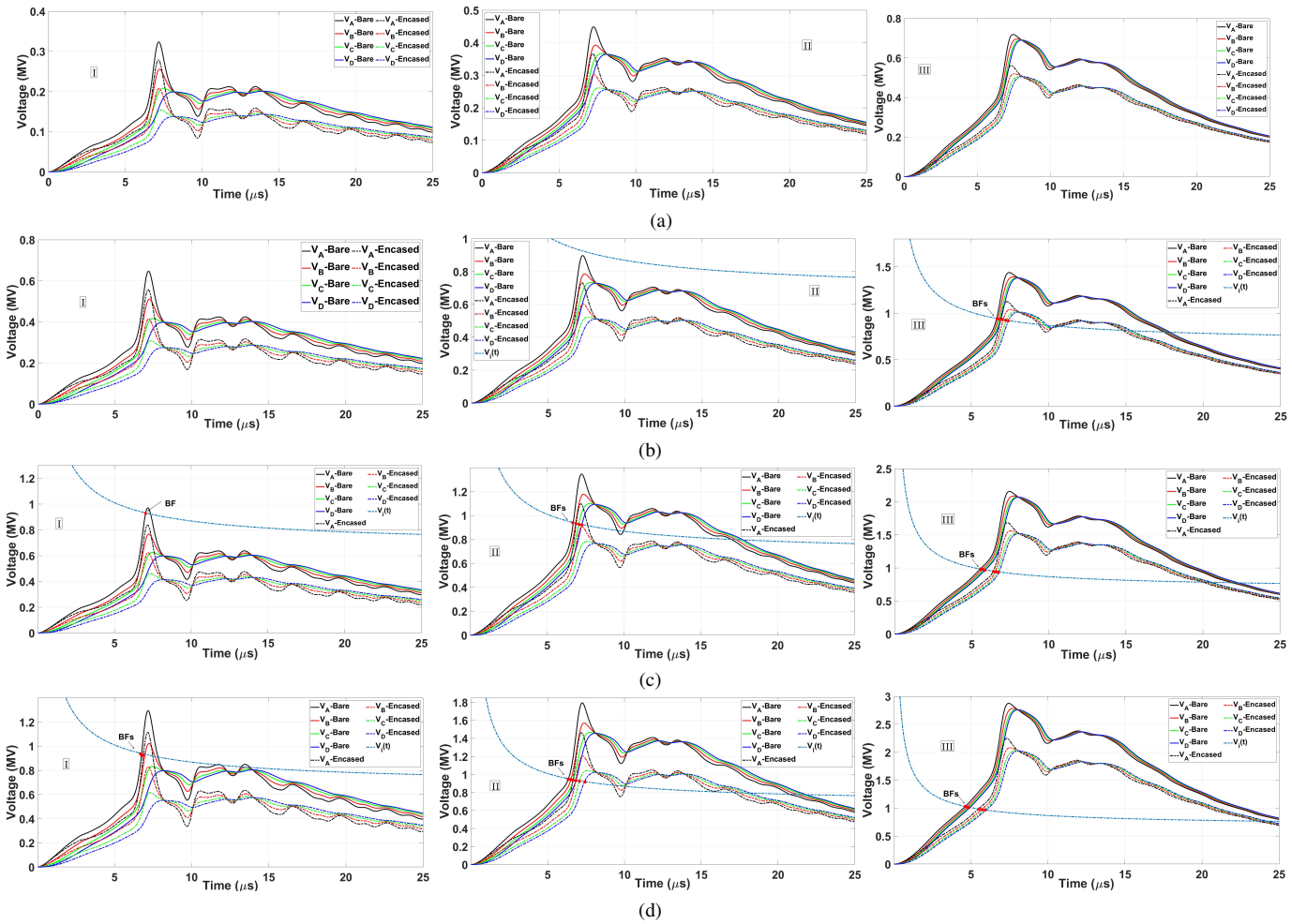

Fig. 6: Comparison of the lightning overvoltages generated at phases A, B and C for soil with ρ_g : $\boxed{I}$ = 700 Ωm, $\boxed{II}$ = 1,500 Ωm, $\boxed{III}$ = 4,000 Ωm; and distinct values of α: (a) α = 0.5; (b) α = 1.0; (c) α = 1.50; (d) α = 2.0

becomes dominant, alternating between inductive and capacitive behavior. The use of concrete significantly reduces the HGI compared to the bare grounding system. Furthermore, Ground Potential Rise (GPR) waveforms exhibit reduced peak values peak values when a concrete-encased grounding system is employed. Additionally, the lightning overvoltages generated in the power system are lower using a concrete-encased grounding system. Consequently, the occurrence of backflashover is diminished compared with that observed with tower-footing grounding system using bare electrodes. These results highlight the potential of concrete as a low-resistivity material to improve the protection of power systems and to mitigate backflashover during transient events in transmission lines.

V. Acknowledgement

Prof. Amauri Gutierrez Martins-Britto is acknowledged for the support and guidance during the implementation of the ULM in the software ATP-EMTP. Prof. Maria Teresa Correia de Barros is acknowledged for having supervised Tainá Pascoalato during her stay as part of a research internship BEPE/FAPESP 2022/09182-3 at IST-University of Lisbon, when implementing the ULM in the ATP-EMTP.

References

[1] G. V. N. Bezerra, F. A. Moreira, T. V. Ferreira, and R. Alipio, "Concrete encased grounding: Lightning response analysis considering the frequency dependence of soil," *IEEE Transactions on Electromagnetic Compatibility*, vol. 66, no. 3, pp. 879–889, 2024.

[2] O. Kherif, S. Robson, H. Griffiths, N. Harid, D. Thorpe, and A. Haddad, "On the high frequency performance of vertical ground electrodes and lrm application," *IEEE Transactions on Electromagnetic Compatibility*, 2024.

[3] M. Daadaa, S. Brettschneider, C. Volat, and G. Simard, "Numerical investigation of the use of electrically conductive concrete-encased electrodes as potential replacement for substation grounding systems," *Energies*, vol. 16, no. 11, 2023. [Online]. Available: https://www.mdpi.com/1996-1073/16/11/4410

[4] L. Grcev, "Modeling of grounding electrodes under lightning currents," *IEEE Transactions on Electromagnetic Compatibility*, vol. 51, no. 3, pp. 559–571, Aug 2009.

[5] M. R. Alemi, S. H. H. Sadeghi, and H. Askarian-Abyaneh, "A marching-on-in-time method of moments for transient modeling of a vertical electrode buried in a lossy medium," *IEEE Transactions on Electromagnetic Compatibility*, vol. 64, no. 6, pp. 2170–2178, 2022.

[6] ——, "A marching-on-in-time method of moments for computation of transient potential rise of grounding grids exposed to lightning strikes," *IEEE Transactions on Electromagnetic Compatibility*, vol. 65, no. 5, pp. 1484–1491, 2023.

[7] Altair-Hyperworks, *Altair Feko*. Altair Engineering, 2023. [Online]. Available: https://altair.com/feko

[8] B. P. Silva, S. Visacro, and F. H. Silveira, "Hem-td: New time-domain electromagnetic model for calculating the lightning response of electric systems and their components," *IEEE Transactions on Power Delivery*, vol. 37, no. 6, pp. 4848–4857, 2022.

[9] ——, "New approaches to represent the frequency dependence of soil parameters on the time-domain hybrid electromagnetic model (hem-td)," *IEEE Transactions on Electromagnetic Compatibility*, vol. 65, no. 6, pp. 1793–1800, 2023.

[10] XGSLab, "Electromagnetic simulation for power, grounding and lightning protection systems." [Online]. Available: https://www.xgslab.com/xgslab-new/general

[11] W. Ye, W. Liu, N. Xiang, K. Li, and W. Chen, "A full-wave peec model for thin-wire structure in the air and homogeneous lossy ground," *IEEE Transactions on Electromagnetic Compatibility*, vol. 65, no. 2, pp. 518–527, 2023.

[12] W. Mingli and F. Yu, "Numerical calculations of internal impedance of solid and tubular cylindrical conductors under large parameters," *IEE Proceedings Generation, Transmission and Distribution*, vol. 151, no. 1, pp. 67–72, 2004.

[13] M. Nakagawa, "Admittance correction effects of a single overhead line," *IEEE Transactions on Power Apparatus and Systems*, no. 3, pp. 1154–1161, 1981.

[14] W. G. CIGRE C4.33, "Impact of soil-parameter frequency dependence on the response of grounding electrodes and on the lightning performance of electrical systems," *Tech. Brochure 781*, pp. 1–66, 2019.

[15] R. Alípio and S. Visacro, "Modeling the frequency dependence of electrical parameters of soil," *IEEE Transactions on Electromagnetic Compatibility*, vol. 56, no. 5, pp. 1163–1171, 2014.

[16] B. Gustavsen and A. Semlyen, "Rational approximation of frequency domain responses by vector fitting," *IEEE Transactions on Power Delivery*, vol. 14, no. 3, pp. 1052–1061, 1999.

[17] M. Ghomi, C. L. Bak, and F. F. da Silva, "Frequency dependence of multilayer soil electrical parameters: Effects on ground potential rise," in *2021 35th International Conference on Lightning Protection (ICLP) and XVI International Symposium on Lightning Protection (SIPDA)*, vol. 1, 2021, pp. 01–08.

[18] J. Colqui, A. de Araújo, C. M. de Seixas, S. Kurokawa, and J. Pissolato Filho, "Performance of the recursive methods applied to compute the transient responses on grounding systems," *Electric Power Systems Research*, vol. 196, p. 107281, 2021. [Online]. Available: https://www.sciencedirect.com/science/article/pii/S0378779621002625

[19] L. Grcev, "Impulse efficiency of ground electrodes," *IEEE Transactions on Power Delivery*, vol. 24, no. 1, pp. 441–451, 2008.

[20] S. Visacro, "The use of the impulse impedance as a concise representation of grounding electrodes in lightning protection applications," *IEEE Transactions on Electromagnetic Compatibility*, vol. 60, no. 5, pp. 1602–1605, 2018.

[21] R. Alipio, M. Guimarães, N. Duarte, and M. T. C. de Barros, "Prompt calculation of tower-footing impulse impedance considering different levels of conservativeness for the frequency dependence of soil parameters," in *2021 35th International Conference on Lightning Protection (ICLP) and XVI International Symposium on Lightning Protection (SIPDA)*, vol. 1. IEEE, 2021, pp. 1–7.

[22] A. De Conti and S. Visacro, "Analytical representation of single- and double-peaked lightning current waveforms," *IEEE Transactions on Electromagnetic Compatibility*, vol. 49, no. 2, pp. 448–451, 2007.

[23] A. J. Oliveira, M. A. O. Schroeder, R. A. R. Moura, M. T. Correia de Barros, and A. C. Lima, "Adjustment of current waveform parameters for first lightning strokes: Representation by heidler functions," in *2017 International Symposium on Lightning Protection (XIV SIPDA)*, 2017, pp. 121–126.

[24] F. O. Zanon, O. E. Leal, and A. De Conti, "Implementation of the universal line model in the alternative transients program," *Electric Power Systems Research*, vol. 197, p. 107311, 2021.

[25] O. E. S. Leal, and , A. De Conti and , F. O. S. Zanon, "User Manual ULM-ATP Version 3.2," accessed October 08, 2024. [Online]. Available: https://github.com/zanonfelipe/ULMAtp

[26] "The ATPDraw Simulation Software (2024), Version 7.5," https://www.atpdraw.net/, accessed: September 13, 2024.

[27] M. A. O. Schroeder, R. A. Moura, F. A. Assis, and J. O. Paulino, "Evaluation of the transmission tower and frequency-dependent soil parameters influence on the grounding potential rise waveforms," *Electric Power Systems Research*, vol. 222, p. 109495, 2023. [Online]. Available: https://www.sciencedirect.com/science/article/pii/S037877962300384X

[28] T. V. Gomes, M. A. O. Schroeder, R. Alipio, A. C. S. de Lima, and A. Piantini, "Investigation of overvoltages in hv underground sections caused by direct strokes considering the frequency-dependent characteristics of grounding," *IEEE Transactions on Electromagnetic Compatibility*, vol. 60, no. 6, pp. 2002–2010, 2018.

[29] A. S. Zalhaf, E. Zhao, Y. Han, P. Yang, A. H. Almaliki, and R. M. Aly, "Evaluation of the transient overvoltages of hvdc transmission lines caused by lightning strikes," *Energies*, vol. 15, no. 4, p. 1452, 2022.

[30] E. Stracqualursi, G. Pelliccione, S. Celozzi, and R. Araneo, "Tower models for power systems transients: A review," *Energies*, vol. 15, no. 13, p. 4893, 2022.

[31] B. Salarieh and B. Kordi, "Full-wave black-box transmission line tower model for the assessment of lightning backflashover," *Electric Power Systems Research*, vol. 199, p. 107399, 2021. [Online]. Available: https://www.sciencedirect.com/science/article/pii/S0378779621003801